A Self-Powered, Biodegradable Dissolved Oxygen Microsensor

Didi She and Mark G. Allen, *Fellow, IEEE*

***Abstract*— We report a biodegradable, self-powered sensor for measurement of dissolved oxygen in the body. The principle of operation is the competition of an oxygen reduction reaction against the ordinarily dominant hydrogen reduction reaction at the cathode of a corroding electrochemical couple. Because the relative contribution of the oxygen reduction reaction to the overall electrochemical reaction depends on the local oxygen concentration, the output voltage of the couple is also dependent on local oxygen concentration. The sensor is formed by embedding the biodegradable metals magnesium and molybdenum within a biodegradable poly(lactic acid) substrate using lamination; external physiological solution is utilized as the electrolyte. The output voltage of the sensor (i.e., the voltage generated across the corroding couple) was measured as a function of oxygen concentration over typical physiological oxygen concentration ranges of 0-60% that of atmospheric oxygen. A linear output voltage response of approximately 6 mV per percentage point oxygen concentration was observed; oxygen concentrations above this range resulted in sensor saturation. [2020-0192]**

***Index Terms*— Battery, biodegradable, corrosion, energy harvesting, oxygen, sensing.**

I. Introduction

OXYGEN-BASED cues can be critical assessments for a wide range of *in vivo* biological effects, ranging from understanding and diagnosing mitochondrial disease [1]–[4] to optimally structuring the microenvironment for cellular growth in tissue engineering and regenerative medicine [5].

In part to address these needs, electrochemical oxygen sensors using microfabrication technologies has been pursued by multiple groups. Many micromachined oxygen sensors are based on the Clark cell, in which the magnitude of the current resulting from the reduction of oxygen in a diffusion-limited operation regime can be correlated to the local oxygen concentration. Clark cells can either utilize interface materials such as Ag/AgCl, which results in an electrochemically stable potential but renders the sensor lifetime relatively short [6]–[11]; or can use noble metals, which have relatively longer lifetime but require cyclic voltammetry for stable output [12]–[14].

These previous micromachined oxygen sensors, as well as their non-micromachined commercial counterparts, are typically made from permanent (non-biodegradable) materials, and also typically require an external power source to drive the electrochemical reaction. A biodegradable oxygen sensor that can break down into non-toxic components after a targeted lifespan, reducing the risk of chronic inflammatory response sometimes observed with permanent devices, is a promising approach to advance the postoperative monitoring of oxygen tension and provide an additional means to monitor a number of diseases and injuries that are transient in nature, such as bone fracture, traumatic brain injury and wound healing. Additionally, such sensors may be useful in environmental monitoring applications, in which widely-dispersed, transient sensors can monitor a large scale system with high spatial fidelity. Examples might include monitoring of plants or crops in precision agriculture applications, or understanding the expanse and evolution of environmental spills or algal tides. The utility of such a device would be further enhanced if it also had a biodegradable power source for both readout and data transfer, such as wireless transmission.

As a first step in addressing these needs we report a biodegradable, self-powered dissolved oxygen sensor. The principle of operation is the competition of an oxygen reduction reaction against the ordinarily dominant hydrogen reduction reaction at the cathode of a corroding electrochemical couple. When the oxygen reduction reaction occurs, there is a shift of the cell potential that correlates to the oxygen availability close to the cathode. This approach allows the measurement of physiological oxygen tension, while simultaneously offering the potential of acting as an energy source for additional devices in an implantable system.

II. Device Concept

The operation of the sensor is based on the competition between two corrosion reactions occurring at the same electrochemical couple; the degree of competition depends on the concentration of dissolved gaseous species proximal to the sensor. Consider, for example, the corrosion of a magnesium-molybdenum (Mg-Mo) galvanic metal pair, embedded in a biodegradable material such as poly(lactic acid) (PLA), and immersed in saline electrolyte as shown in Fig. 1. Note that these metals have been demonstrated

Manuscript received May 15, 2020; revised June 25, 2020; accepted June 29, 2020. Date of publication September 14, 2020; date of current version October 7, 2020. This work was supported in part by the National Institutes of Health under Grant 5R21AR066322 and in part by the National Science Foundation (NSF) National Nanotechnology Coordinated Infrastructure Program under Grant NNCI-1542153. Subject Editor R. Ghodssi. *(Corresponding author: Didi She.)*

Didi She was with the University of Pennsylvania, Philadelphia, PA 19104 USA. She is currently with Google, Inc., Mountain View, CA 94043 USA (e-mail: shedidi1990@gmail.com).

Mark G. Allen is with the Singh Nanotechnology Center, University of Pennsylvania, Philadelphia, PA 19104 USA (e-mail: mallen@seas.upenn.edu).

Color versions of one or more of the figures in this article are available online at http://ieeexplore.ieee.org.

Digital Object Identifier 10.1109/JMEMS.2020.3013208

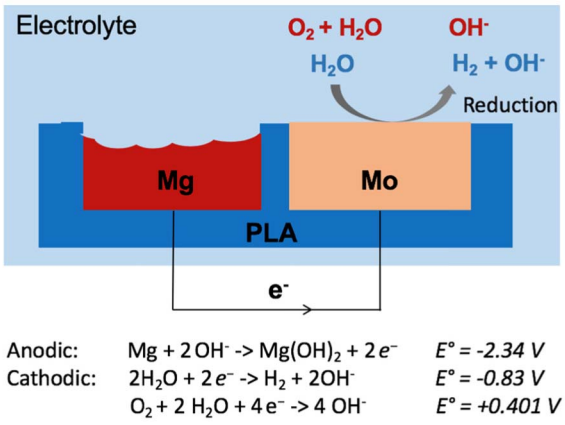

Fig. 1. A corroding Mg-Mo couple immersed in saline electrolyte and forming an electrochemical cell. Two competing reactions at the cathode will result in a shift in the cell potential depending on the concentration of oxygen in the electrolyte.

to be biodegradable, and have been utilized previously as biodegradable batteries [15].

In such a corroding couple, electrical energy can be derived from the spontaneous galvanic protection of Mo through the anodic oxidation of Mg. Considering such a system as an electrochemical cell, oxidation of Mg takes place on the anode surface as follows:

$$Mg \rightarrow Mg^{2+} + 2e^- \tag{1}$$

At the cathode of the electrochemical cell, hydrogen evolution occurs:

$$2H_2O + 2e^- \rightarrow H_2 + 2OH^- \tag{2}$$

However, if oxygen is present, a competing oxygen reduction reaction can also take place at the cathode:

$$O_2 + 2H_2O + 4e^- \rightarrow 4OH^- \tag{3}$$

Ultimately, magnesium hydroxide is formed from the following reaction:

$$Mg^{2+} + 2OH^- \rightarrow Mg(OH)_2 \tag{4}$$

A competing side reaction also takes place at the anode and forms hydrogen gas and magnesium hydroxide simultaneously:

$$Mg + 2H_2O \rightarrow Mg(OH)_2 + H_2 \tag{5}$$

In an oxygen-poor environment, the oxygen reduction reaction cannot occur, and the developed anode-cathode potential is reflective of the hydrogen evolution reaction. However, in the presence of oxygen, the oxygen reduction reaction can occur and compete with the hydrogen evolution reaction, resulting in a variation of the output potential of the corroding couple. As will be demonstrated, the output potential exhibits an approximately linear dependence on oxygen concentration until the oxygen reduction reaction dominates the hydrogen evolution reaction, at which point saturation behavior is observed.

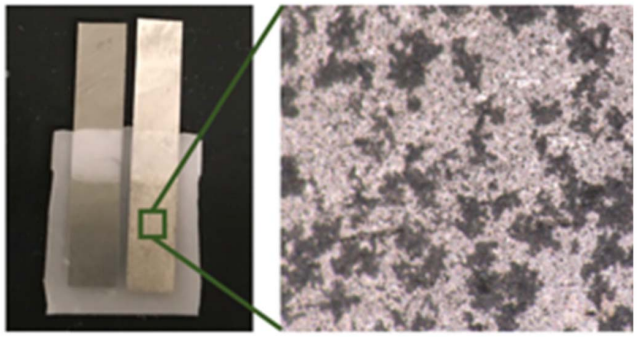

Fig. 2. Photomicrograph of a fabricated oxygen sensor. (Left) – fabricated Mg and Mo strips embossed into PLA substrate. (Right) – Close view of Mg surface showing the formation of a passivating $Mg(OH)_2$ film upon initiation of corrosion.

III. Device Fabrication

A proof-of-concept biodegradable oxygen sensor was fabricated using lamination and embossing technologies developed for previous biodegradable sensors using dissolving metals and biodegradable polymers [16]. Briefly, Mg and Mo foils approximately 50 microns in thickness were laser-patterned into strips approximately 4.5mm wide, and embossed into a 200 micron thick substrate of poly(lactic acid) (PLA). The lateral extent of the substrate was 15mm × 18mm, and the lateral separation between foils was approximately 1mm. The surface of the substrate was then optionally passivated with additional PLA such that an active area of 0.45 cm^2 for each electrode was exposed. A cross-sectional schematic of the devise structure is shown in Fig. 1, and a photomicrograph of a fabricated cell is shown in Fig. 2.

IV. Electrochemcial Behavior

To further understand the competition between possible reactions in this system, potentials between the Mg and Mo electrodes, as well as the potentials between individual electrodes and a Ag/AgCl standard, were investigated. Due to mass transfer limitations, measurement of potentials at relatively high currents can be taken as a proxy for reduced oxygen concentration in the proximity of the sensor, since oxygen is consumed in the oxygen reduction reaction. Fig. 3 shows galvanodynamic measurements (potential vs. current density) of these three electrode cases taken at a scan rate of 0.01 $mA/cm^2 \cdot s$. Given the relative invariance of Mg vs Ag/AgCl to scan rate, the overall Mg/Mo cell voltage change is mainly attributed to the characteristics of current dependence of the cathodic reaction. Specifically, the cathode (Mo) electrode potential vs. Ag/AgCl exhibits a decrease from approximately −0.2V to −1V for current densities ranging from 0 to 0.45 mA/cm^2, followed by a plateau at higher current densities. The observed potential in this range is lower than the oxygen reduction potential (0.179 V vs. Ag/AgCl) and higher than the hydrogen evolution potential (−1.05 V vs. Ag/AgCl), suggesting that both types of reactions could take place. The cathodic reaction shifts completely to hydrogen evolution (−1.2 to −1.3 V vs. Ag/AgCl) at higher current densities, together with a significant increase of the amount of

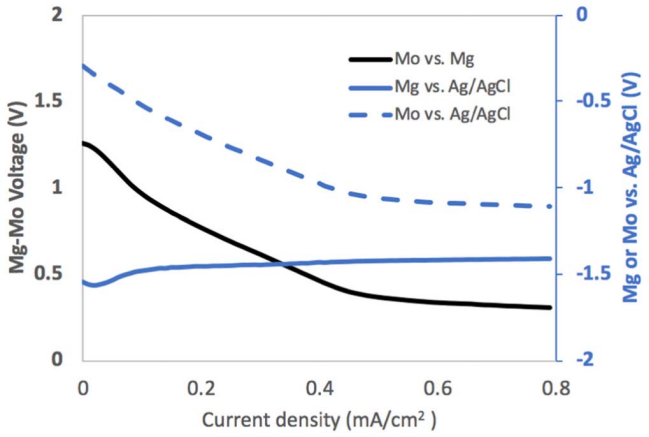

Fig. 3. Galvanodynamic measurements of the Mg-Mo electrode pair (left scale) as well as the individual Mg and Mo electrodes vs. Ag/AgCl (right scale) as a function of current density. Measurements were performed at a scan rate of 0.01 mA/cm^2·s.

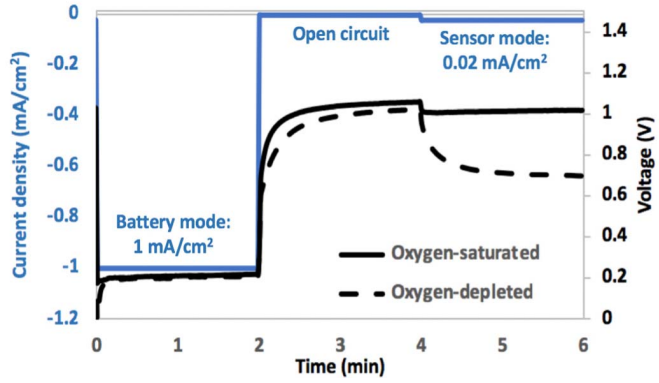

Fig. 4. Operation diagram of the oxygen sensor versus time. (1) The sensor is operated in battery mode at high current density to remove the effect of anode passivation. (2) The sensor is rested in open circuit mode to allow the oxygen concentration to re-equilibrate with the embedding environment. (3) The sensor is operated in sensor mode at low current density. If significant oxygen is present in the embedding environment, the sensor potential remains relatively high; however, if oxygen is depleted in the embedding environment, the potential will fall.

visible hydrogen generation at the cathode. These observations are consistent with an operating hypothesis of a change in the dominant cathodic reaction from oxygen reduction to hydrogen evolution.

V. Device Operation

Although the oxygen sensitivity of the output potential results from the competition of cathodic reactions, reactions at the anode cannot be ignored. In particular, the anodic reaction forms a passivation layer of $Mg(OH)_2$ at the Mg surface (Fig. 2), and continued discharge relies on the continuous formation and breakdown of this passivation layer. When sufficiently high current is drawn from the electrochemical cell, the $Mg(OH)_2$ layer is mechanically disrupted to expose the underlying magnesium. However, the data presented in Fig. 3 indicate that oxygen sensing should take place at relatively low current densities. As the current density decreases, the rate

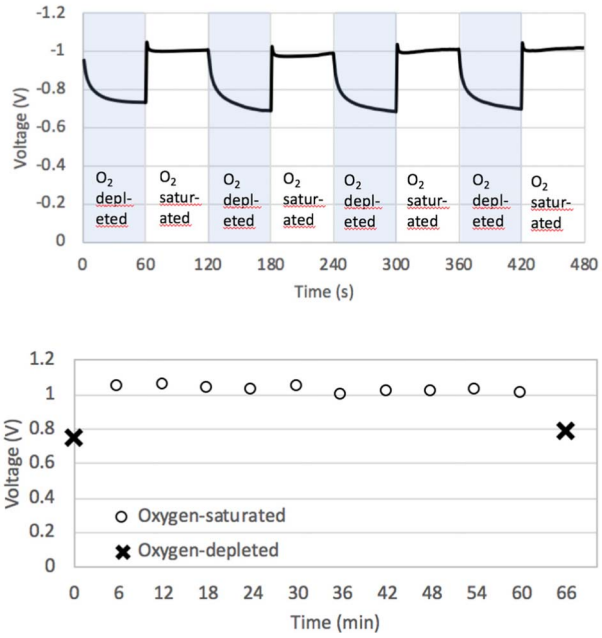

Fig. 5. (Top) The output voltage of the sensor in cycled environments of oxygen-depleted (shaded) and oxygen-saturated (non-shaded) environments as a function of time. In constructing Fig. 5, the sensor was operated as described in Fig. 4, and the sensor mode portions of the Fig. 4 response were stitched together to better compare cycles side-by-side. (Bottom) Stability measurement of the sensor as the sensor is held in an oxygen-saturated solution. Sensor sensitivity is validated by measuring in an oxygen-depleted state before and after the stability test.

of $Mg(OH)_2$ reformation exceeds the rate of film breakdown, which subsequently leads to an increase in internal resistance.

To ensure stable operation of the sensor (high current discharge) as well as the ability to detect oxygen (low current discharge), the device is operated in two modes: 'battery mode' and 'sensor mode'. As shown in Fig. 4, in battery mode a relatively high current density (1 mA/cm^2) is drawn from the device to induce breakdown of any passivating $Mg(OH)_2$ surface film and ensure a relatively constant anode surface area; while in sensor mode, the current density is reduced 50-fold to 0.02 mA/cm^2, allowing the oxygen reduction reaction to play an important role. To overcome mass-transfer limitations of oxygen consumption at the cathode during 'battery mode' operation, a two-minute open-circuit recovery step is inserted between anode regeneration and cathode measurement to allow the oxygen concentration in the vicinity of the sensor to re-equilibrate with the embedding environment. The voltage in the plateau region during 'sensor mode' is taken as a measure of the oxygen concentration in the embedding environment.

The reproducibility and stability of the sensor to an electrolyte environment with varying oxygen concentrations was assessed as shown in Fig. 5. In the upper portion of Fig. 5, the sensor was alternately immersed in an oxygen-depleted electrolyte and an oxygen-rich electrolyte. The sensor responses of each cycle are compared side-by-side, and showed comparable performance as each environment was alternated. In the lower portion of Figure 5, a sensor stability test was performed, in which the output voltage of the sensor was first measured in an oxygen-depleted electrolyte, and the sensor was then

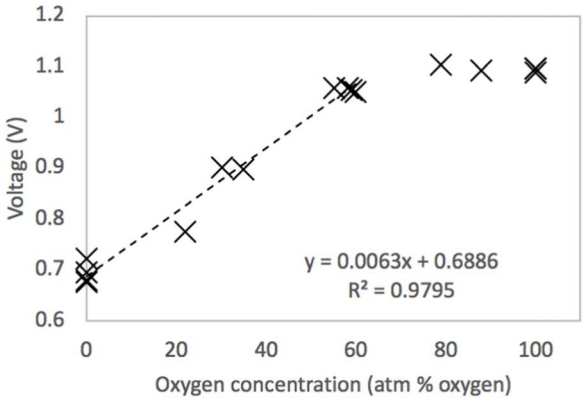

Fig. 6. Sensor output voltage as a function of oxygen concentration in the electrolyte corrected for atmospheric concentration (100 atm% oxygen corresponds to normal concentration of oxygen in air) at a discharge rate of 0.02 mA/cm^2. A linear plus saturation response is observed.

held in an oxygen-saturated environment. The output voltage fluctuation over a timespan of one hour is within ±5%. After removal from this saturated electrolyte, the sensor retains its functionality and oxygen sensitivity, as demonstrated by its subsequent ability to sense in an oxygen-depleted electrolyte.

To further validate the performance of the sensor, the sensor output voltage at a discharge current density of 0.02 mA/cm^2 in a 0.1M NaCl aqueous electrolyte environment was assessed against a commercial fiber-optic oxygen sensor probe (MicrOx TX3, PreSens) immersed in the same environment. The oxygen content of the environment was modified by addition of sodium sulfite to the solution [17]; the slow sulfite-sulfate oxidation reaction consumed oxygen in the solution and allowed for a decreasing oxygen concentration in the electrolyte as a function of time that could be simultaneously measured by both the biodegradable sensor and the commercial oxygen sensor. Fig. 6 shows the correlation between the two sensors. Over the physiologically-relevant range of 0-60 atm% oxygen, the biodegradable sensor exhibits reasonable linearity, with a sensitivity of approximately 6 mV/atm% oxygen.

VI. Conclusion

A self-powered chemical sensor made of biodegradable materials has been presented. This sensor demonstrates the utility of combining biodegradable batteries, in which corroding electrochemical couples of biodegradable metals in saline can produce electrical energy for implantable systems, with electrochemical sensors that operate by exploiting the effect of the measurand on the output voltage of these corroding couples. The use of differing metal couples may result in output voltages of different ranges, enabling the opportunity to sense other measurands with differing electrochemical potentials. Further, the ability to operate this sensor both in battery mode and sensor mode offers the possibility to build more complex implantable systems that can sense other physical and chemical parameters of interest, using the battery mode of the sensor as a power supply for other sensors.

The sensitivity and dynamic range of the sensors can be adjusted by changing the measurement conditions and geometry of the sensor. The sensors presented here were optimized to the typical physiological range of 0-60 atm%. However, operation of the sensor at different current densities in sensor mode, or adjusting the sensor geometry, could be exploited to focus on other oxygen sensor ranges of interest.

The selectivity of these sensors to measurands other than oxygen was not assessed. When considering *in vivo* applications, selectivity benefits from the tightly controlled homeostatic conditions within the body. For example, the major gases present in blood are oxygen and carbon dioxide, and pH is tightly controlled [18]. However, when considering more expansive applications such as environmental monitoring in which confounding measurands may be present, the selectivity of this approach should be examined. If required, selectivity enhancement approaches such as the incorporation of thin gas-selective coatings over the sensors [19], [20], or the use of differential measurements to remove common-mode factors such as temperature, could be considered.

The sensors presented here were not operated in an *in vivo* environment; instead, they were assessed in controlled environments on the laboratory bench in a wired fashion. In order to realize fully implantable devices with wireless communication, integration of the voltage output with a voltage-to-frequency conversion circuit could be considered. Even simple circuits such as ring oscillators could be utilized, either constructed in vanishingly-small silicon, or using organic electronics.

Acknowledgment

Microfabrication and testing was carried out at the Singh Center for Nanotechnology at the University of Pennsylvania. The authors would like to acknowledge valuable technical discussions with Dr. Robert Guldberg, Dr. Nicholas Willett, Dr. Zarazuela Cunningham, Dr. Marni Falk, Dr. Douglas Wallace, and Dr. Melissa Tsang on application scenarios of interest for this class of sensors.

References

[1] P. Venditti, L. Di Stefano, and S. Di Meo, "Mitochondrial metabolism of reactive oxygen species," *Mitochondrion*, vol. 13, no. 2, pp. 71–82, Mar. 2013.

[2] J. Park, T. Bansal, M. Pinelis, and M. M. Maharbiz, "A microsystem for sensing and patterning oxidative microgradients during cell culture," *Lab Chip*, vol. .6, no. 5, pp. 611–622, 2006.

[3] I. G. Kirkinezos and C. T. Moraes, "Reactive oxygen species and mitochondrial diseases," *Seminars Cell Develop. Biol.*, vol. 12, no. 6, pp. 449–457, 2001.

[4] A. Carreau, B. E. Hafny-Rahbi, A. Matejuk, C. Grillon, and C. Kieda, "Why is the partial oxygen pressure of human tissues a crucial parameter? Small molecules and hypoxia," *J. Cellular Mol. Med.*, vol. 15, no. 6, pp. 1239–1253, Jun. 2011.

[5] B. S. Klosterhoff *et al.*, "Implantable sensors for regenerative medicine," *J. Biomechanical Eng.*, vol. 139, no. 2, Feb. 2017, Art. no. 0210091.

[6] H. Suzuki, T. Hirakawa, I. Watanabe, and Y. Kikuchi, "Determination of blood PO_2 using a micromachined clark-type oxygen electrode," *Anal. Chim. Acta*, vol. 431, no. 2, pp. 249–259, Mar. 2001.

[7] H. Suzuki, "Microfabrication of chemical sensors and biosensors for environmental monitoring," *Mater. Sci. Eng., C*, vol. 12, nos. 1–2, pp. 55–61, Aug. 2000.

[8] H. Suzuki, H. Ozawa, S. Sasaki, and I. Karube, "A novel thin-film AG/AGCl anode structure for microfabricated clark-type oxygen electrodes," *Sens. Actuators B, Chem.*, vol. 53, no. 3, pp. 140–146, Dec. 1998.

[9] H. Suzuki, H. Arakawa, and I. Karube, "Fabrication of a sensing module using micromachined biosensors," *Biosensors Bioelectron.*, vol. 16, nos. 9–12, pp. 725–733, Dec. 2001.

[10] C.-C. Wu, H.-N. Luk, Y.-T.-T. Lin, and C.-Y. Yuan, "A clark-type oxygen chip for *in situ* estimation of the respiratory activity of adhering cells," *Talanta*, vol. 81, nos. 1–2, pp. 228–234, Apr. 2010.
[11] M. Wittkampf, G.-C. Chemnitius, K. Cammann, M. Rospert, and W. Mokwa, "Silicon thin film sensor for measurement of dissolved oxygen," *Sens. Actuators B, Chem.*, vol. 43, nos. 1–3, pp. 40–44, Sep. 1997.
[12] J. Park, Y. K. Pak, and J. J. Pak, "A microfabricated reservoir-type oxygen sensor for measuring the real-time cellular oxygen consumption rate at various conditions," *Sens. Actuators B, Chem.*, vol. 147, no. 1, pp. 263–269, May 2010.
[13] C.-C. Wu, T. Yasukawa, H. Shiku, and T. Matsue, "Fabrication of miniature clark oxygen sensor integrated with microstructure," *Sens. Actuators B, Chem.*, vol. 110, no. 2, pp. 342–349, Oct. 2005.
[14] D. She and M. G. Allen, "A micromachined freestanding electrochemical sensor for measuring dissolved oxygen," *J. Microelectromech. Syst.*, vol. 28, no. 3, pp. 521–531, Jun. 2019.
[15] L. Yin *et al.*, "Materials, designs, and operational characteristics for fully biodegradable primary batteries," *Adv. Mater.*, vol. 26, no. 23, pp. 3879–3884, Jun. 2014.
[16] M. Luo, A. W. Martinez, C. Song, F. Herrault, and M. G. Allen, "A microfabricated wireless RF pressure sensor made completely of biodegradable materials," *J. Microelectromech. Syst.*, vol. 23, no. 1, pp. 4–13, Feb. 2014.
[17] S. Kikuchi, K. Honda, and S. Kim, "Removal of dissolved oxygen by sodium Sulfite. Application to the polarographic study," *Bull. Chem. Soc. Jpn.*, vol. 27, no. 1, pp. 65–68, Jan. 1954.
[18] A. Bacher, "Effects of body temperature on blood gases," *Intensive Care Med.*, vol. 31, no. 1, pp. 24–27, Jan. 2005.
[19] P. Althainz, A. Dahlke, M. Frietsch-Klarhof, J. Goschnick, and H. J. Ache, "Reception tuning of gas-sensor microsystems by selective coatings," *Sens. Actuators B, Chem.*, vol. 25, nos. 1–3, pp. 366–369, Apr. 1995.
[20] D. Lin and Y. Zhao, "Innovations in the development and application of edible coatings for fresh and minimally processed fruits and vegetables," *Comprehensive Rev. Food Sci. Food Saf.*, vol. 6, no. 3, pp. 60–75, Jul. 2007.

Didi She received the B.S. degree in electrical engineering from Southeast University, Nanjing, China, in 2011, the M.S. degree in microelectronics and solid-state electronics from Peking University, Beijing, China, in 2014, and the Ph.D. degree in electrical and systems engineering from the University of Pennsylvania in 2019. She is currently a Staff Engineer at Google. Her research interests focused on the exploration of novel implantable devices for MEMS applications.

Mark G. Allen (Fellow, IEEE) received the B.A. degree in chemistry, the B.S.E. degree in chemical engineering, and the B.S.E. degree in electrical engineering from the University of Pennsylvania, Philadelphia, and the S.M. and Ph.D. degrees from the Massachusetts Institute of Technology, Cambridge. In 1989, he joined the Faculty of the School of Electrical and Computer Engineering, Georgia Institute of Technology, Atlanta, ultimately holding the rank of Regents' Professor and the J.M. Pettit Professorship in microelectronics, as well as a joint appointment with the School of Chemical and Biomolecular Engineering. In 2013, he left Georgia Tech to become the Alfred Fitler Moore Professor of Electrical and Systems Engineering and the Scientific Director of the Singh Nanotechnology Center, University of Pennsylvania. His research interests include the development and the application of new micro- and nanofabrication technologies, as well as MEMS. He is a co-founder of multiple MEMS companies, including Cardiomems, Axion Biosystems, and EnaChip. He received the IEEE 2016 Daniel P. Noble Award for contributions to research and development, clinical translation, and commercialization of biomedical microsystems. He was the Co-Chair of the 1996 IEEE Microelectromechanical Systems Conference, the 2012 Power MEMS Conference, chaired the 2016 Solid State Sensors, Actuators, and Microsystems Conference ('Hilton Head'), and was previously the Editor-in-Chief of the *Journal of Micromechanics and Microengineering*.